Pergamon

Chemical Engineering Science, Vol. 50, No. 2, pp. 183 199, 1995

0009-2509/95 $9.50 + 0.00

0009-2509(94)00225-8

BUBBLE-TRAIN FLOW IN CAPILLARIES OF CIRCULAR AND SQUARE CROSS SECTION

T. C. THULASIDAS, M. A. ABRAHAM and R. L. CERRO†
Department of Chemical Engineering, The University of Tulsa, Tulsa, OK 74104-3189, U.S.A.

(*Received* 19 *August* 1993; *accepted in revised form* 23 *July* 1994)

Abstract—Ceramic monoliths first developed for their use in automotive catalyst, are used now to perform three-phase, catalyzed reactions. The large mass transfer rates achieved within this type of reactor are the result of large interfacial area and very thin diffusion paths. These enhanced mass transfer rates are credited to the presence of well-developed bubble-train flow. Bubble-train flows consist of trains of long bubbles separated by liquid slugs. The interfacial area is the area of the bubbles and the thin films are the result of the squeezing action of the bubbles as they overtake the liquid slugs. The objective of this paper is to predict the main mass transfer parameters, such as bubble size and shape, bubble velocity, and volume fraction of gas inside capillaries of circular or square cross section, on the basis of the superficial flow rates of gas and liquid in the feed. Experiments are reported here on bubble train flow inside capillaries of circular and square cross section for a large range of capillary numbers. A mass balance model was developed to allow the computation of flow parameters using an iteration scheme.

1. THE MONOLITH HONEYCOMB AS A THREE-PHASE REACTOR

The monolith honeycomb structure is widely known for its application as catalyst support in the field of automotive emissions control. This structure consists of an array of parallel, straight, uniform, non-connecting square channels from one to a few millimeters in size and is made of ceramic materials, i.e. cordierite. Recently a new application was introduced; monolithic structures are being used as catalyst support for carrying out multiphase reactions. Satterfield and Ozel (1977) analyzed the potential advantages of using monolithic structures as catalyst reactors in lieu of conventional packed bed reactors. The advantages are mainly (1) low pressure drop, (2) good gas–liquid contacting and better liquid distribution (3) minimum axial dispersion and high effectiveness factor and (4) higher flow rates for comparable reactor volumes. The lack of radial transport, however, may be a disadvantage for exothermic reactions. Several applications of monolith structures as support for catalytic reactions have been reported. Benoit and Kohler (1975) found that monolith structures are suitable for use as enzyme support in continuous tubular reactors. Agira *et al.* (1986) used monoliths for immobilization of *Escherichia coli* in reactions with and without gas evolution. Kawakami *et al.* (1989) used monoliths to immobilize an enzyme, glucose oxidase, for the oxidation of glucose. Gas–liquid and liquid–solid mass transfer rates were measured both for upward flow and downward flow conditions. Mass transfer rates for upward flow were found to be much higher than that for downward flow, yet both rates were higher than the rates found in a trickle bed reactor. Irandoust and Gahne (1990) performed hydrodesulfurization and hydrogenation reactions over Co–Mo/γAl_2O_3 catalyst impregnated on the walls of the monolith. More recently (Shah *et al.*, 1993; Crynes *et al.*, 1993) a monolith was used as a catalyst support in the oxidation of phenol.

The key to the good performance of monoliths as three-phase catalyzed reactors rests on the ability to attain a steady bubble-train flow. Obtaining a good distribution of gas and liquid inside the channels of the monolith, however, has remained the biggest challenge. The work described here was designed to provide a fundamental understanding of the mechanics of bubble-train flows in the cells of monoliths used as catalyst support in a novel three-phase reactor with applications in wastewater treatment and other chemical reactions. The novelty of the system developed at The University of Tulsa is based on the fact that gas and liquid are fed to the monolith as a froth to produce bubble-train flow inside the monolith channels. This method, unlike feeding methods used by other researchers, can be used to feed industrial-size reactors.

2. BUBBLE-TRAIN FLOWS INSIDE CAPILLARIES

The flow of two fluid phases in pipes and capillaries share a few common features. In pipes and capillaries alike, the actual velocities of the two fluid phases are related to the volume fraction of the phases inside the domain of flow. The volume fraction of the fluid phases are related in a complex way to the phase average velocities. There are, however, qualitative differences stemming from the fact that inside capillaries, capillary forces play a major role. Flow in capillaries are essentially laminar and predominantly viscous, the liquid slugs are free of smaller bubbles and breakage and coalescence of bubbles is largely absent.

†Author to whom correspondence should be addressed.

Bubble-train flow consists of trains of long bubbles separated by liquid slugs flowing concurrently inside a capillary with circular or square cross section. Long bubbles have lengths that are several times the diameter of the capillary. The term *very long bubble* is reserved here for experiments where the *bubble* forms with the back end open. The term bubble-train flow is used to emphasize the capillary nature of this flow as opposed to the, mostly inertial, slug flows found in large pipes. When long bubbles move inside capillaries, otherwise filled with a wetting liquid, they are surrounded by a very thin film of liquid that flows under the pull of gravity. The thickness of the surrounding film is a function of the bubble velocity and, for fluids of low viscosity, is typically 5–50 μm thick. Mass transfer from the gas to the walls of the capillary is enhanced by the increased interfacial area and by the very short diffusion path. The films are continuously renewed by the movement of the bubbles and by the mixing that takes place inside the liquid slugs.

Fairbrother and Stubbs (1935) performed experiments to determine liquid flow rates through capillaries by the movement of an indicator bubble. They noticed that bubbles moved faster than the liquid due to the presence of the liquid film surrounding the bubble. A simple empirical relationship was suggested for their experiments

$$W = \frac{U_b - v_{ls}}{U_b} = 1.0\,(Ca)^{1/2}, \quad 7.5 \times 10^{-5} < Ca < 0.014 \tag{1}$$

where U_b is the velocity of the bubble, v_{ls} is the mean liquid velocity and Ca is the Capillary number. The Capillary number is defined as $Ca = \mu_l U_b/\sigma$, where μ_l is the viscosity of the liquid and σ is the interfacial tension. Marchessault and Mason (1960) measured the thickness of the liquid film surrounding the air bubbles inside circular capillaries in different fluids, using a conductimetric technique and proposed the following correlation for the film thickness

$$\frac{R - R_b}{R} = -0.05\left(\frac{\mu_l}{\sigma}\right)^{1/2} + 0.89\,Ca^{1/2}, \quad 7 \times 10^{-6} < Ca < 2 \times 10^{-4} \tag{2}$$

where R_b is the radius of the bubble and R is the radius of the capillary tube. The constant in the first term to the right of eq. (2) has units of $(\text{cm/s})^{1/2}$. Taylor (1961) using a refined version of Fairbrother and Stubbs (1935) experimental method reported values of the relative bubble velocity, W, for a wide range of Ca and found an asymptotic limit of $W = 0.56$ at large Ca. Bretherton (1961) used lubrication theory to carry out a detailed analysis of the movement of bubbles in circular capillaries. Bretherton's solution for small Ca predicts values of the relative velocity slightly smaller than Fairbrother and Stubbs (1935)

$$W = 1.29\,(3\,Ca)^{2/3}. \tag{3}$$

Bretherton estimated the accuracy of eq. (3) to be within 5% if $Ca < 0.003$ and within 10% if $Ca < 0.005$. For vertical tubes, Bretherton introduced a correction to eq. (3) using a factor of $1 \pm \frac{2}{3}\,Bo$ for upward and downward flow, respectively. The Bond number is defined as the ratio of gravity to capillary forces, $Bo = \varrho_l g R^2/\sigma$, where ϱ_l is the density of the liquid and g is the acceleration due to gravity. This correction is the first term of a series expansion and is valid for small values of the Bond number. Gravity affects the velocity of the liquid film flowing down in the film surrounding the bubble and the curvature of the static meniscus. Bretherton (1961) measured the film thickness by noting the change in length of a liquid slug moving at constant speed in a circular capillary. His experimental results showed systematic deviation from eq. (3) at lower Ca—derived based on the assumption of low Ca—but found no satisfactory explanation for this behavior. The film thickness obtained for upward flow was found to be very close to that for horizontal flow. Bretherton also predicted, based on a static equilibrium of forces, that the bubble will not rise due to the effect of gravity through stationary liquid in a vertical tube sealed at one end if the $Bo < 0.842$. Cox (1962) solved numerically the fourth-order equations for the streamline function of the fluid surrounding the bubble and presented experimental data indicating that the limit for large Ca of $W = 0.6$. In a later paper Cox (1964) obtained the experimental confirmation of the streamline patterns in front of the bubble as proposed by Taylor (1961).

Goldsmith and Mason (1963) studied the movement of bubbles and liquid drops inside circular capillaries. They measured film thickness using a travelling microscope for a range of $0.01 < Ca < 0.2$. These results agreed very well with Taylor's (1961) experimental results. Teletzke (1983) augmented Bretherton's theory by introducing surface tension gradients, disjoining pressure, and lack of perfect slip into the original lubrication approximation analysis. He predicted that the film thickness will level off to an equilibrium value at the limit of very small Ca and that the thickness of the wetting film will increase with an increase in the viscosity ratio (μ_1/μ_2) where μ_1 is the viscosity of displacing fluid and μ_2 is the viscosity of displaced fluid. Chen (1986) reported experimental data for the thickness of the film surrounding air bubbles and oil drops in water for a wide range of Ca and showed that the liquid film thickness levels off to an equilibrium value at lower Ca as predicted by Teletzke. The liquid film thickness surrounding air bubbles, however, was found to be larger than the film surrounding oil drops, contrary to Teletzke's theory. Schwartz *et al.* (1986) examined the liquid film surrounding air bubbles of varying length in water. They found that for very small Ca the liquid film thickness depend on the length of the bubble as well as the Ca. Herbolsheimer (1987) and later Ratulowski and Chang (1990) suggested an explanation for this phenomena and also for some of the experimental discrepancies found by Bretherton (1961), based on the effect of impurities on the surface tension of newly created surfaces.

When a bubble is introduced in a stationary liquid contained in a tube sealed at one end, the bubble will rise through the liquid, due to gravity, only if the Bond number, $Bo \geqslant 0.842$ (Bretherton, 1961). Reinelt (1987) obtained a numerical solution for this problem using a finite difference method and compared it to the perturbation solution obtained by Bretherton (1961). Recently, Pozrikidis (1992) analyzed this problem for drops of immiscible liquids when the viscosity of the drops is identical to the viscosity of the surrounding liquid.

Several numerical solutions describing the flow of bubbles and liquids in capillaries have been reported in the literature. Reinelt and Saffman (1985) reported a finite difference solution for the motion of bubbles in channels and circular tubes. Shen and Udell (1985) reported the results from a finite element study. Martinez and Udell (1989) reported a boundary integral analysis of the same problem. Ratulowski and Chang (1989) used Bretherton's (1961) approach and solved the lubrication equations in an arc length–angle coordinate system and extended the validity of the solution for larger Ca.

The analysis of movement of bubbles and liquid slugs inside a square tube have not been done until recently. Ratulowski and Chang (1989) included computation of axisymmetric bubbles in square capillaries using a Galerkin spectral technique to find the flow coefficients. Detailed experimental investigation about the motion of very long bubbles in square capillaries were reported by Kolb and Cerro (1991, 1993a) in association with the coating of monolithic structures. Experimental diameters of bubbles in the axial and diagonal planes and streamline patterns in front of the bubbles were reported in these studies as well as numerical computations for bubble diameter based on an analytic solution of the flow of a film in the space between a circular bubble and a square capillary (Kolb and Cerro, 1993b). The limitations on this analysis are imposed by the fact that the bubble is not axisymmetric at $Ca \leqslant 0.10$ and the possible breakdown of the lubrication approximation at $Ca \geqslant 0.60$.

For tubes larger than a few centimeters in diameter, inertial and gravity forces play a larger role and the effect of capillarity is very small. Davies and Taylor (1950) developed an expression for bubbles moving inside tubes when inertia and gravity are important and capillarity is negligible. The rise velocity of the bubble under these conditions can be expressed as the velocity of gravity waves

$$U_b = 0.328\sqrt{gD} \tag{4}$$

where D is the diameter of the tube. If the liquid in the tube is not stationary, a correction is needed to account for the velocity of the liquid

$$U_b = C_1 v_{ls} + C\sqrt{gD} \tag{5}$$

where C_1 is a constant. Collins *et al.* (1978) developed an approximate solution for the flow of bubbles in large tubes for both laminar and turbulent flow of liquid as given below:
For laminar flow:

$$U_b = 2.27\ v_{ls} + 0.361\ (gD)^{1/2}. \tag{6}$$

For turbulent flow:

$$U_b = 1.2\ v_{ls} + 0.35\ (gD)^{1/2}. \tag{7}$$

It is evident from eqs (5)–(7) that the bubble moves faster than the liquid. The first term to the right of eqs (5)–(7) accounts for the movement of the liquid and the second term accounts for the independent movement due to gravity waves. Experimental results confirm these observations. Bendikson (1985) improved upon Collins theory by including surface tension terms in the analysis.

3. HYDRODYNAMIC MODEL FOR BUBBLE-TRAIN FLOW IN CAPILLARIES

A hydrodynamic model for bubble-train flow inside capillaries of circular and square cross section is discussed here. The purpose of this analysis is to integrate in a continuum model the discrete nature of the motion of bubbles and liquid slug in order to predict bubble velocities, liquid film thickness and volume fraction of liquid and gas inside the cells with the knowledge of measurable macroscopic quantities such as the superficial gas and liquid velocities.

In a circular tube a bubble can be approximated as having a cylindrical body with two nearly hemispherical caps. In a square tube, the profile of the bubble may be more complex. At large Ca, bubbles inside capillaries of square cross section, are axisymmetric (Kolb and Cerro, 1991) and the approximation used for circular capillaries is also valid. For small Ca, bubbles inside square capillaries are not axisymmetric. See Fig. 1(a) and (b). The cross section of the middle body of a bubble is approximated by flat films on the side regions and constant curvature liquid lenses in the corners. The ends of the bubbles are more complex and the caps are three-dimensional with the exception of the regions near the tip where the surface is again a sector of a sphere. For a long bubble, that is a bubble length that is several times the diameter of the capillary, most of the gas flow rate is accounted by the body of the bubble. As a consequence, the actual shape of the bubble cap has little effect on the total volumetric gas flow rate.

A train of bubbles and liquid slugs move concurrently in horizontal, upward or downward motion, inside a capillary. Since there are no breakage or coalescence of bubbles, the bubbles and slugs move at the same apparent velocity. The volume of the bubbles may change slightly due to the change in hydrostatic pressure and mass transfer from the bubble to the surrounding liquid, but there is no convective flow in or out of the bubbles. The liquid slugs on the other hand, are continuously receiving liquid from the slugs upstream and sending liquid to the slugs downstream. Bubbles and liquid slugs can have different lengths. Assume that at any given time

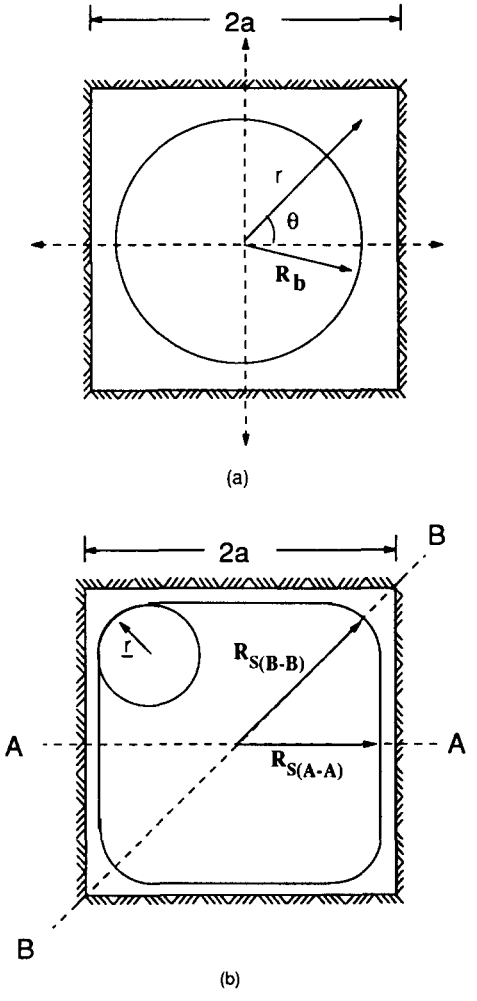

Fig. 1. Schematic view of the cross section of bubble inside a square capillary: (a) axisymmetric bubble, (b) non-axisymmetric bubble.

all the bubbles have the same length and that their length is several times the diameter of the capillary. Similarly, all liquid slugs are assumed to have the same length. The basic element of this analysis is a cell consisting of one bubble and one liquid slug, as shown in Fig. 2. A long bubble has a body that may or may not be axisymmetric and two end caps. The cross-sectional area of the body of the bubble is A_b and A is the cross-sectional area of the capillary. The liquid surrounding the body of the bubble flows down under the effect of gravity regardless of the direction of movement of the bubble. The flow rate of liquid in the film surrounding the bubble will be shown to depend on the film thickness and the physical properties of the liquid, for both circular and square capillaries. Assuming that the bubble caps are hemispheres of diameter d_b, the length of the bubble is equal to the sum of the length of the body of the bubble, l_b, plus the diameter d_b. The total length of the unit element is: $l_T = l_b + l_s + d_b$, where l_s is the length of the liquid slug defined from the tip of the upstream bubble to the tip of the downstream bubble.

Assume that the liquid flows around the hemispherical caps with velocity profiles similar to a falling film with varying thickness and free surface velocities but constant flow rate. This assumption is consistent with a macroscopic mass balance in a control volume that encloses the bubble. In the liquid slugs the velocity profiles are parabolic with average velocity v_{ls}. Consider a control volume ABCD, attached to the capillary, as shown in Fig. 2. Liquid flows into the control volume through the surface AB. Liquid flows in and gas flows out of the control volume through surface CD. Assuming incompressible fluids, continuity gives

$$A_b U_b = A v_{ls} + q_{lf} \tag{8}$$

where q_{lf} is the liquid flow rate in the film between the capillary wall and the bubble. Equation (8) relates the bubble velocity with the velocity of the liquid in the slug and in the surrounding film.

The movement of the unit cell consisting of one bubble and one liquid slug depends on the relative velocities of bubbles and liquid slugs. It will take a unit cell a time t_T to cross the plane AB, stationary with respect to the walls of the capillary, and it will take a bubble time t_b to cross the plane AB,

$$t_T = \frac{l_T}{U_b}, \quad t_b = \left(\frac{l_b + d_b}{U_b}\right). \tag{9}$$

Since the volume of a bubble is given by

$$V_g = \left(A_b l_b + A_b \frac{2}{3} d_b\right) \tag{10}$$

the superficial gas velocity, J_g, that is the gas flow rate per unit area of the capillary is given by

$$J_g = \frac{A_b U_b}{A l_T}\left[l_b + \frac{2}{3} d_b\right]. \tag{11}$$

In a similar way, an expression for the superficial liquid velocity can be obtained by taking into account the time that a liquid slug takes to cross the plane AB, $t_s = (l_s/U_b)$. The total volume of liquid that crosses plane AB is given by

$$V_l = A v_{ls} \frac{l_s}{U_b} + \frac{\pi d_b^3}{12} - q_{lf} \frac{l_b + d_b}{U_b} \tag{12}$$

where it is assumed that both phases are moving upward. Notice that the liquid flow rate in the film surrounding the bubble is negative, since the film is flowing down due to the effect of gravity. The superficial liquid velocity is given by

$$J_l = \frac{U_b}{A l_T}\left(A v_{ls} \frac{l_s}{U_b} + \frac{\pi d_b^3}{12} - q_{lf} \frac{l_b + d_b}{U_b}\right) \tag{13}$$

where the second term on the right of eq. (13) represents the volume of liquid contained between the spherical bubble cap and a cylinder with the same radius and height than the bubble cap. Equations (8), (11) and (13) can be simplified to get

$$J = J_l + J_g = v_{ls} \tag{14}$$

where J is overall superficial flow rate, defined as the

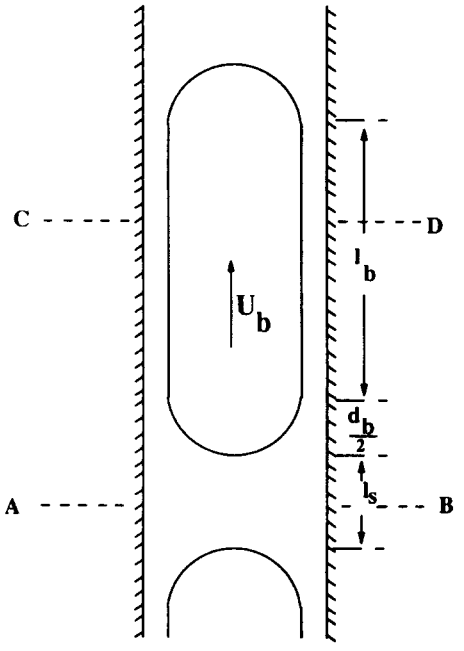

Fig. 2. Schematic of unit cell with one bubble and one liquid slug inside a capillary.

sum of the gas and liquid superficial velocities. Equations (8) and (14) can be combined to give a relationship linking the bubble velocity to the overall superficial velocity;

$$A_b U_b = A J + q_{lf}. \tag{15}$$

The area of the bubble is a function of the capillary number in a non-trivial way. The flow rate of the surrounding liquid film, q_{lf}, can be estimated assuming that it is a fully developed gravity flow. On the cylindrical body of the bubble, curvature of the free surface and hence the pressure field are constant and forces generated by the acceleration of gravity are balanced by viscous stresses on the solid surface. Even when there is an externally imposed pressure field driving the bubble-train flow upwards, the liquid film surrounding the cylindrical body of the bubble, flows down due to gravity. The boundary conditions for this flow are; no slip at the capillary wall and zero shear stresses on the bubble surface. For circular capillaries, the velocity profile for the film flow is given by (Reinelt, 1987)

$$v_z = \frac{\varrho_l g R^2}{4\mu_l}\left[1 - \left(\frac{r}{R}\right)^2 + 2\left(\frac{R_b}{R}\right)^2 \ln\left(\frac{r}{R}\right)\right]. \tag{16}$$

The flow rate of the liquid film surrounding the bubble, q_{lf}, is obtained after integration over the cross section of the falling film

$$q_{lf} = \frac{\pi \varrho_l g R^4}{8\mu_l}\left[1 + 4\left(\frac{R_b}{R}\right)^4 \left[\frac{3}{4} - \ln\left(\frac{R_b}{R}\right) - \left(\frac{R_b}{R}\right)^{-2}\right]\right]. \tag{17}$$

For square capillaries, a solution for the film flow surrounding a circular bubble inside a square tube was developed recently by Kolb and Cerro (1993b) using an infinite series. The film flow rate, q_{lf}, obtained after integration of the velocity profile in the region enclosed by the circular bubble and the square capillary can be adequately represented by a fifth-order polynomial

$$q_{lf} = \frac{\varrho_l g a^4}{8\mu_l}[4.499 + 0.09528\ R_s - 16.21\ R_s^2 + 9.216\ R_s^3 + 8.566\ R_s^4 - 6.09\ R_s^5] \tag{18}$$

where R_s is the dimensionless bubble radius. The coefficients shown in eq. (18) are more accurate and are slightly different from the coefficients reported by Kolb and Cerro (1993b) for a third-order polynomial. The characteristic length in this formulation is one half the length of the side of the square capillary. There is no similar expression for the liquid flow rate in the case of a square capillary and a non-axisymmetric bubble. However, this flow rate can be approximated by combining the velocity profile for a circular bubble in a square capillary at the corners, with a flat falling film on the sides. The geometric construction shown in Fig. 1 was done assuming that the interface of the non-axisymmetric bubble at the corners of the square capillaries is an arc with constant curvature. For a non-axisymmetric bubble, flow in the corners of the capillary accounts for more than 95% of the total flow rate. (Kolb and Cerro, 1993b). This approximate velocity profile and the flow rate obtained by integration are compared satisfactorily with a numerical solution obtained using a finite element package, FIDAP from Fluid Dynamics International, Evanston, IL.

The volume fraction of gas inside the capillary at any instant of time is another important parameter in the description of bubble-train flows in tubes and capillaries. The volume fraction of gas, α, defined as the volume of the bubbles inside the capillary divided by the total volume of the capillary, can be shown to be given by (Wallis, 1969)

$$\alpha = \frac{J_g}{U_b}. \tag{19}$$

Introducing the relationship relating the bubble velocity with the length of the bubble and the total length of the unit cell, eq. (11), gives

$$\beta = \alpha \frac{A}{A_b} + \frac{d_b}{3 l_T} \tag{20}$$

where β is the ratio of the length of a bubble to the length of the unit cell. In capillaries, the second term on the right of eq. (20), $(d_b/3l_T)$, is very small, except for very short bubbles and slugs, and may be neglected. This results in a simple relationship between the volume fraction of gas, α, and the ratio of the length of the bubbles to the length of the unit cell, β.

Equations (15)–(20), and an empirical (or theoretical) relationship between the bubble velocity, U_b, and

the bubble cross sectional area, A_b, allow the prediction of the main macroscopic flow properties, such as volume fraction of gas inside the capillaries, velocity of the bubbles and ratio of bubble length to liquid slug length from the knowledge of gas and liquid flow rates. The cross-sectional area of the bubble as a function of bubble velocity, or better yet as a function of Capillary number, is a complex relationship involving the momentum balance and the Young–Laplace equation as the boundary condition for the normal stresses at the gas–liquid interface. This relationship is known through experimental data and from the solution of the momentum balance first developed by Bretherton (1961) and more recently by Reinelt (1987), Ratulowski and Chang (1989), and Kolb and Cerro (1993a).

4. EXPERIMENTAL SET-UP

Figure 3 is a schematic representation of the experimental apparatus used for bubble-train flow visualization and measurement. It consists of three parts, namely, (1) the viewing cell, (2) the liquid and gas feed systems, and (3) the image analysis system. The viewing cell encloses the capillaries of circular or square cross section. A 2 mm borosilicate square capillary and a 2 mm precision bore capillary tubing (Wilmad Glass corp., Buena, NJ) were used in the experiments. The capillaries, 0.305 m long, are enclosed in a 0.038 m inner diameter acrylic tube and then filled with glycerine. By matching the refractive index of borosilicate glass with glycerine, refraction of light at the outer wall of the capillary is avoided. Two flat windows on opposite sides of the tube are made by cutting the acrylic tube sides and pasting microscope glass slides. These windows are needed to avoid distortions in all measurements that involve length. The capillaries are positioned coaxially within the acrylic tube.

A steady train of bubbles and liquid slugs is created outside the capillary in a polypropylene tee from separate gas and liquid feeds. By carefully controlling the gas and liquid flow rates a steady stream of gas bubbles and liquid slugs with nearly uniform sizes could be created for most of the flow rates studied here. Average values of bubble and liquid slugs were taken for the few cases where uniform distribution was hard to achieve. Constant liquid flow was generated using a syringe pump. Air flow to the tee was controlled by a combination of two metering valves and a small chamber (volume 352 cc) placed between them. The first valve regulates flow from the air cylinder which is at high pressure while the second valve does a finer control of flow from the chamber to the tee. A pressure transducer indicates the pressure inside the chamber. Since the viewing cell was opened to atmosphere, this pressure reading is the total pressure

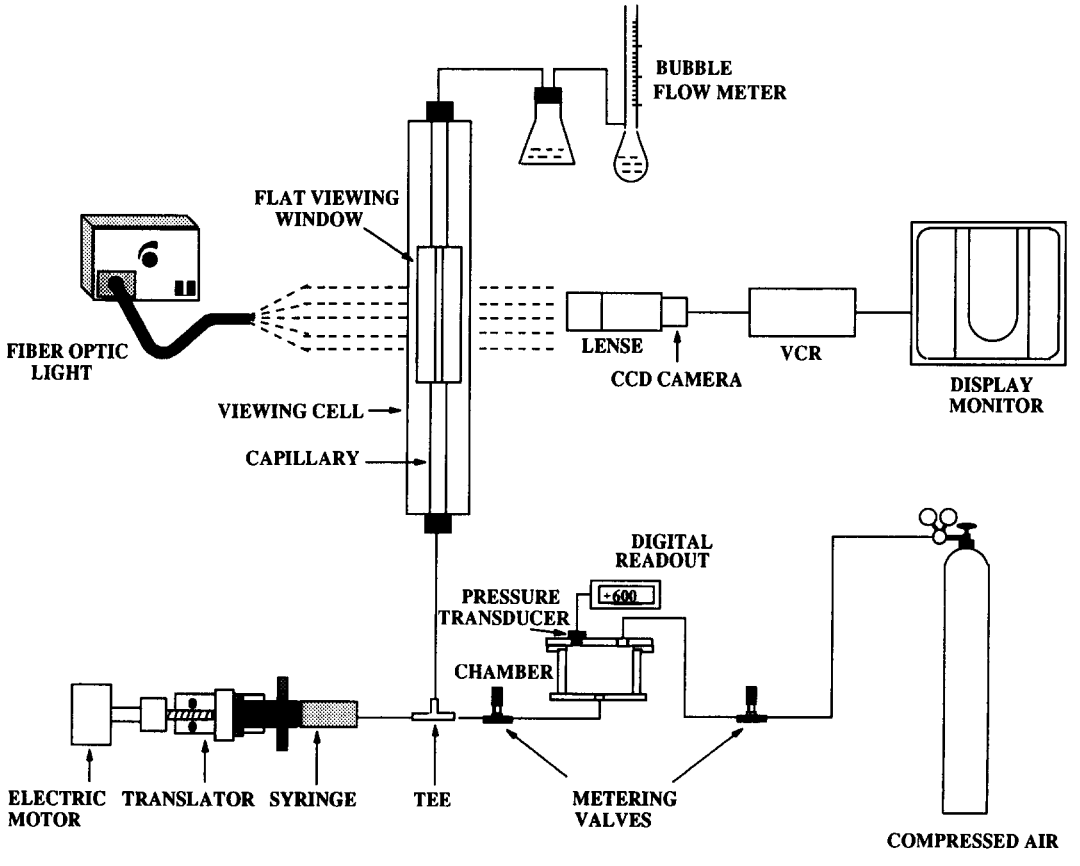

Fig. 3. Schematic view of experimental set-up.

drop in the line including that from fittings. The liquid flow rate was measured from the calibrated syringe pump feed and the total flow rate through the capillary was measured at the exit using a bubble flow meter. The gas flow rate was taken as the difference between the total and liquid flow rates, in effect neglecting any expansion of the gas volume inside the capillary. This can be justified on the grounds that most of the pressure drop occurs in the flow control fittings.

The flow visualization system includes lighting, image sensing and recording equipment. Direct measurement of the velocity of the bubble from the video display monitor was made possible using two independent image sensing and recording systems. The first system is a color CCD camera, IK – C30A (Toshiba) with shutter speeds of 1/60 or 1/1000 and a Panasonic AG – 7300 cassette recorder. This recorder is capable of recording images at a rate of 30 frames per second. The maximum velocity that could be measured by this system is only a few centimeters per second (0.04–0.05 m/s). For the highest range of bubble velocities a Kodak Ektapro-EM high speed video imaging system was used. This processor is capable of recording images up to 1000 frames per second with a variable shutter speed. Two lenses were used, Nikkor 55 mm micro with a PK-13 extension ring and the D.O industries zoom 6000 microscopic. Fiber optic back lighting provided satisfactory illumination of the capillary and the gas–liquid interface. The images were stored in a video cassette for later analysis. A Sony PVM-2530 was used as the display monitor.

For very long bubble experiments, this experimental set-up was modified to include a small reservoir chamber at the entrance and a ball valve and a metering valve at the exit (see Fig. 4.) The capillary is filled from the bottom at a slow rate to remove all the air from the system. Once the capillary is filled with liquid, the ball valve is closed, the metering valve is kept partially open and the chamber is pressurized with air. The cell is then placed in upflow, horizontal, or downflow position. At this point the exit valve is opened suddenly and the bubble is allowed to travel the length of the capillary. A large volume of the chamber compared to that of the capillaries, ensures a constant driving force.

Silicone oil (dimethyl polysiloxane from Sigma Chemical Co, St. Louis, MO) and water were used as liquids and air as gas here. The choice of silicone oil was influenced by the fact that, it is a transparent Newtonian fluid, available in a wide range of viscosities, immiscible with air and maintains constant physical properties. Using three different oils with viscosities 0.0046, 0.048 and 0.971 Pa s, a wide range of Capillary numbers were covered. The densities of

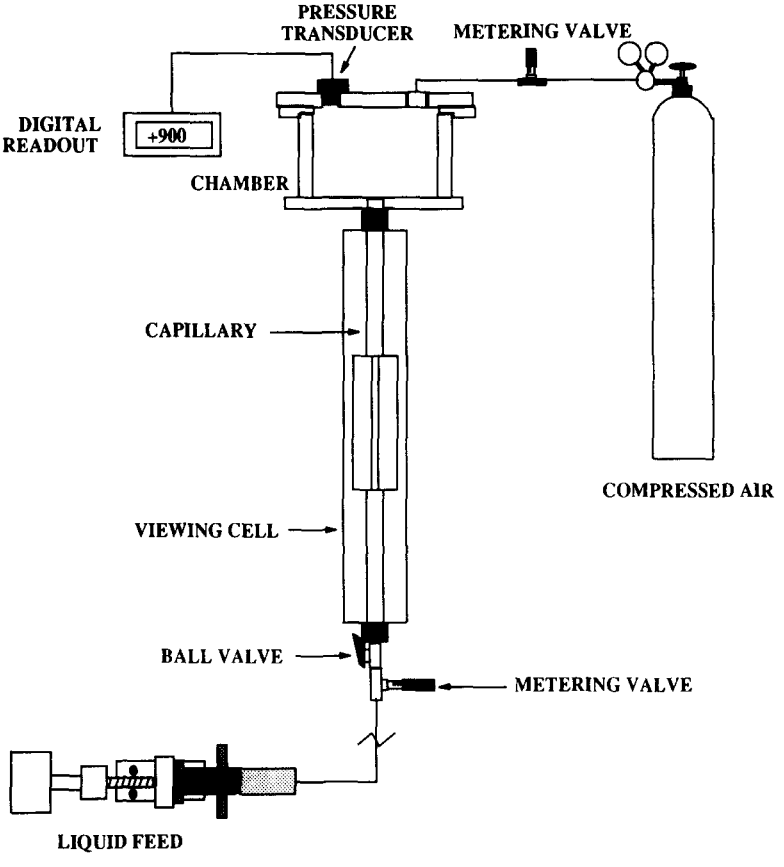

Fig. 4. Close-up view of experimental set-up for very long bubbles.

these oils are 913, 957 and 971 kg/m^3, respectively. The main difficulty encountered with the use of silicone oil was the cleaning of capillaries. This was overcome by employing chromic-sulfuric solution for cleaning and then drying with air. Ultrapure water was also used in all water experiments. The interfacial tensions of both liquids were determined by the pendant drop method (Ramos *et al.*, 1993). Typical surface tensions for silicone oil and water were 22.18 and 71.86 mN/m, respectively. The difference in refractive indices of air ($n_D = 1.0$) and silicone oil ($n_D = 1.403$) or water ($n_D = 1.33$) resulted in significant scattering of light at the gas–liquid interface. A correction for refraction of light at the solid–fluid interfaces was made following the procedure outline by Kolb and Cerro (1991).

All measurements were made directly from the display monitor. A scaling factor for these measurements was obtained by placing an objective micrometer in the field of view. The variables measured from the display monitor are lengths of bubbles and slugs, velocity, and diameter of the bubbles. The velocity of bubbles were determined by measuring the distance travelled for a few frames on the display monitor. The bubble interface as displayed on the monitor was slightly distorted due to the refraction of light. The magnitude of this error, however, was found to be negligible (less than 2%). In addition, a very small error is introduced by the limiting resolution of the monitor. Assuming the error is one pixel on each side of the bubble, the maximum error is about 0.6% for a 2 mm capillary. During experiments performed at high liquid and gas flow rates it was not possible to maintain uniform bubble and liquid slug sizes. For these experiments, average values were determined from a large number of measurements.

The shape of a bubble in a vertical, circular capillary is always axisymmetric. The shape of bubbles in square capillaries are axisymmetric for large *Ca* and non-axisymmetric for low *Ca*. Non-axisymmetric bubbles are flattened out at the sides of the capillary, leaving a very thin liquid film in the flat region and a liquid pool in the corner region. For the computation of bubble volumes and liquid flow rates in the film surrounding the bubbles, the shape of non-axisymmetric bubbles is defined by connecting flat films with arcs of constant radius at the corners. The radius of the arc at the corners as well as the cross-sectional area of the bubble are known from the radius of the bubble in the axial and diagonal planes (Kolb and Cerro, 1991).

5. RESULTS AND DISCUSSION

Bubble diameters in circular and square capillaries

Dimensionless bubble diameters for the 2 mm circular capillary as a function of Capillary number are shown in Fig. 5. Three orders of magnitude changes of *Ca*, $0.004 \leqslant Ca \leqslant 3$ are covered here. Most of the upper range of *Ca* was covered with silicone oil of viscosity 0.971 Pa s while the lower range was covered with an oil of viscosity, 0.048 Pa s, with an intermediate overlapping region. As indicated, these experimental results cover upward, downward, and horizontal flow of very long bubbles as well as upward flow of bubble-trains. Taylor's (1961) experimental results are shown as a full line.

Cox (1962) found a slight discrepancy with Taylor's result and reported non-axisymmetric horizontal

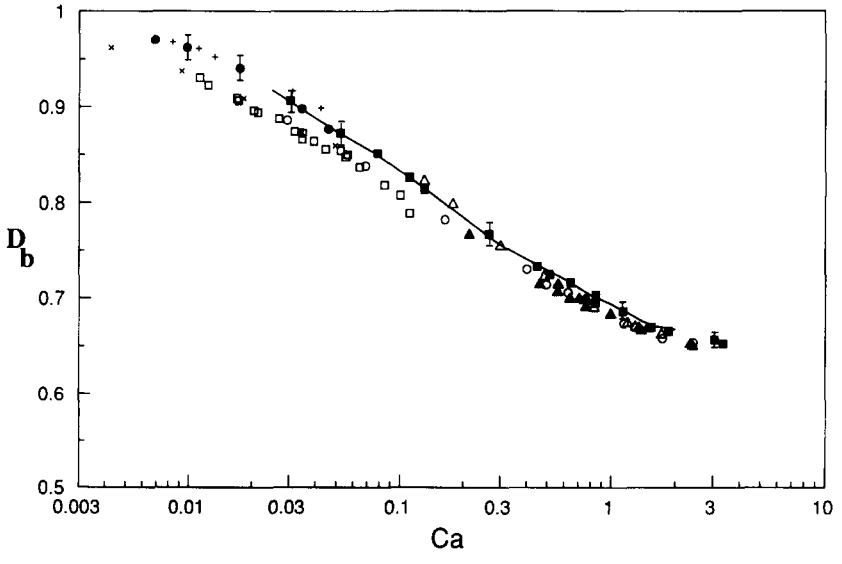

Fig. 5. Dimensionless bubble diameter as a function of Capillary number for circular capillaries: (■) 1000 centistokes silicone oil, horizontal flow; (○) 1000 centistokes silicone oil, upward flow; (△) 1000 centistokes silicone oil, downward flow; (▲) 1000 centistokes silicone oil, bubble-train flow; (●) 50 centistokes silicone oil, horizontal flow; (×) 50 centistokes silicone oil, upward flow; (+) 50 centistokes silicone oil, downward flow; (□) 50 centistokes silicone oil, bubble-train flow. The solid line represents Taylor (1961) experimental results. Error bounds have been included on some of the experimental points.

bubble shapes due to the effect of gravity. This effect was observed in the experiments reported here, for the cases where the capillary was placed horizontally. The results presented here for horizontal flow closely follow Taylor's (1961) results. The effect of gravity on the bubble motion is evident in Fig. 5. For Ca greater than 0.3, the differences in D_b for upward flow and downward flow are negligible. At large Ca, viscous forces are dominant and the effect of gravity is minimized. In the lower Ca range, however, the upward flow and downward flow lines bifurcate. For upward flow, at the lowest experimental Ca, the liquid film thickness was found to be almost twice that for horizontal flow whereas for downward flow and horizontal flow the bubble diameter are almost undistinguishable. Bretherton's (1961) prediction, using the correction factor $(1 \pm \frac{2}{3}Bo)$ amounts to a liquid film only 1.28 times thicker or thinner than the thickness of the horizontal flow. The Bond number in these experiments was $Bo = 0.43$, that is not in the range where it would be negligible. It may be argued that Bretherton's theory would be only qualitatively applicable here. There are, however, discrepancies between these experiments and Bretherton's predictions that must be pointed out. For horizontal flows and $Ca \geqslant 0.3$, where viscous forces are dominant, the diameter of bubbles in horizontal flow are larger than the diameters found for both upward and downward flow. At low Ca, on the other hand, the horizontal and downward flow diameters are almost identical. Numerical solutions, where gravity is neglected (Martinez and Udell, 1989; Reinelt and Saffman, 1985) agree well with Taylor's and the results presented here for horizontal flow.

Marangoni effects (Herbolzheimer, 1987; Ratulowski and Chang, 1990) could be used to explain discrepancies between experiments and theory or between similar experiments performed with different fluids. Most of the experiments reported here, however, are at a range of Ca larger than the range where Marangoni effects can be important. Differences between experimental values for horizontal vs upward or downward flow, can be found for the largest range of Capillary numbers ($Ca \approx 1$).

The diameter of bubbles in upward bubble-train flow closely follows that for very long bubbles in upward flow. For bubbles at least 2 or 3 times the diameter of the capillary, the mechanism determining the bubble diameter is a balance of forces at the leading end of the bubble only. Hence, it is expected that any theoretical analysis applicable for very long bubbles will be equally applicable for trains of bubbles as long as the length of the bubble is several times larger than the diameter of the capillary. The maximum bubble velocity recorded in these experiments was 0.051 m/s, corresponding to a Reynolds number, $Re = 2.04$, and Bond number, $Bo = 0.43$.

Dimensionless bubble diameter for the 2 mm square capillary are shown in Fig. 6. Included are the diameter of long bubbles in upward and downward flow as well as train of bubbles in upward flow. No horizontal flow experiments were done in square capillaries as gravity effects are much more pronounced. Three silicone oils and water were used for a wide range of Capillary numbers, $10^{-4} \leqslant Ca \leqslant 4$. These results are compared with the experimental data reported by Kolb and Cerro (1991) for downward flow at high Ca. At low Ca, bubbles become non-axisymmetric with flat sides and liquid lenses at the corners. In these experiments, the diameter of the bubbles were measured in the axial and diagonal planes and transition was recorded as the Ca where both diameters became equal. Kolb and Cerro (1991) performed most experiments at $Ca > 0.1$ and recorded the transition at $Ca \approx 0.1$. In this work a large number of experiments were performed for upward flow around the transition point that has been determined with more accuracy, to take place at $Ca = 0.04$. Remarkably, the transition to occur at $Ca = 0.04$ was predicted by the numerical computations of Ratulowski and Chang (1989). This transition point is important while undertaking a theoretical analysis of the bubble motion in that, different approaches are required for these two different regions. As was the case with circular capillaries, at lower Ca the effect of gravity is more pronounced. The thickness of the liquid film surrounding the bubble in the axial and diagonal planes for upward flow were found to be higher than that for downward flow. The same effect was observed in the circular experiments. For $Ca \leqslant 0.01$, the thickness of the liquid film in the axial plane is very thin and hard to measure by direct observation. As a consequence only the diameter of the bubble in the diagonal plane is reported for the smallest range of Ca. Currently, an experimental method based on Moire interferometry is being tested for the measurement of the very thin film thickness in the axial plane. The liquid film in the axial plane is very thin but has not been drained completely of liquid as could be expected from the pressure gradient generated by the free surface curvature at the corners. Experiments for bubble train flow of water and air are also reported in the very low Ca range. For upward flow, the diameter of the bubbles in the diagonal plane for the water–air system are larger than the diameter of bubbles for the silicone oil–air system in upward flow. This behavior, as was already pointed out by Chen (1986), does not agree with Teletzke's (1983) prediction of a larger film for increasing viscosity ratio. In these experiments the maximum Reynolds number for the water–air system is $Re = 862.3$, and inertial forces may not be negligible.

Relative bubble velocities for circular and square capillaries

Bubbles always move faster than the liquid slugs, regardless of the direction of flow. The extent of the relative velocity of the bubble with respect the average velocity of the liquid slugs depends on the bubble diameter and the direction of flow. Using the relationship obtained from the macroscopic mass balance, eq.

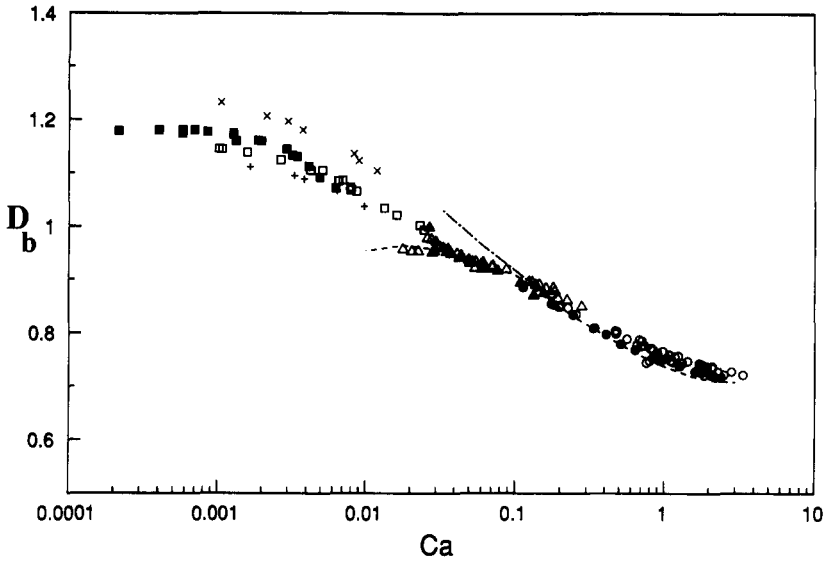

Fig. 6. Dimensionless bubble diameter as a function of Capillary number for square capillaries; (●) 1000 centistokes silicone oil, downward flow. (○) 1000 centistokes silicone oil, bubble-train flow; (▲) 50 centistokes silicone oil, upward flow; (△) 50 centistokes silicone oil, bubble-train flow; (+) 5 centistokes silicone oil, upward flow; (×) 5 centistokes silicone oil, downward flow; (□) 5 centistokes silicone oil, bubble-train flow; (■) water, bubble-train flow; (– –) Kolb and Cerro (1991) experimental results in the axial plane. (—) Kolb and Cerro (1991) experimental results in the diagonal plane.

8, the relative velocity is given by

$$W = \frac{A - A_b}{A} \pm \frac{q_{lf}}{A U_b} \tag{21}$$

where the plus sign in the last term is valid for upward flow, the minus sign is valid for downward flow and the term is zero in horizontal flow. The ratio of the cross-sectional areas is a measure of the amount of liquid film left behind by the bubble, while the term on the right is the gravity flow of liquid that for upwards flow increases the velocity differential while for downward flow decreases it.

Figure 7 shows values of W calculated from experimental data for circular capillaries, for a very large range of Ca, $10^{-6} \leqslant Ca \leqslant 10$. Experimental results reported here are for upward, downward, and horizontal flow for the range $10^{-3} < Ca < 3$. The results from different workers shown as different lines in Fig. 7, includes all known experimental and theoretical data. Most of the experimental results available in the literature are for horizontal capillaries. There is considerable scatter in the experimental data reported for low Ca. One of the causes of this spread of data is the fact that the liquid film surrounding the bubbles became extremely thin, only a few microns in size. The data from Marchessault and Mason (1960) are consistently higher than other's experimental results. The empirical correlations found by Fairbrother and Stubbs (1935) predicts values of W smaller than Marchessault and Mason's data but larger than Chen's (1986) and Schwartz *et al.* (1986). Bretherton's (1961) correlation, consistently predicts values of W smaller than any available data, Chen's experimental data show different values of W for the water–air system than for the water–oil system, indicating a dependence on the viscosity ratio that is not contemplated by Bretherton's theory. Notably, Chen's experimental data of W for the water–oil system as well as the water–air system, levels off at low Ca as predicted by Teletzke (1983) while none of the other's data shows a similar behavior. Experimental results reported here for horizontal flow agree with Fairbrother and Stubbs (1935) empirical correlation only for a small range of Ca. The effect of gravity is evident for the low Ca range, where the relative velocity for upward flow is larger than the relative velocity for downward flow. Experimental results shown here reach the limiting value of $W \to 0.58$ for large Ca. The largest Ca for these experiments, however, is only $Ca = 3.03$. Data reported by Goldsmith and Mason (1963) in the range $0.01 < Ca < 0.10$ is not shown in Fig. 7, but agrees very well with the results shown here for horizontal flow.

Values of W calculated from experimental data for the square capillary are shown in Fig. 8. The relative velocity, as shown by Kolb and Cerro (1991) approaches asymptotically a limiting value of $W = 0.60$ at higher Ca. To understand the large difference in relative velocities found for upward and downward flows at low Ca, it is necessary to take into account the large contribution of the corners to the total flow rate. For downward flow, W decrease continuously when the Ca is reduced and becomes zero. For upward flow, on the other hand, W decreases continuously with decreasing Ca, reaches a minimum value and then increases again. The minimum value of W is

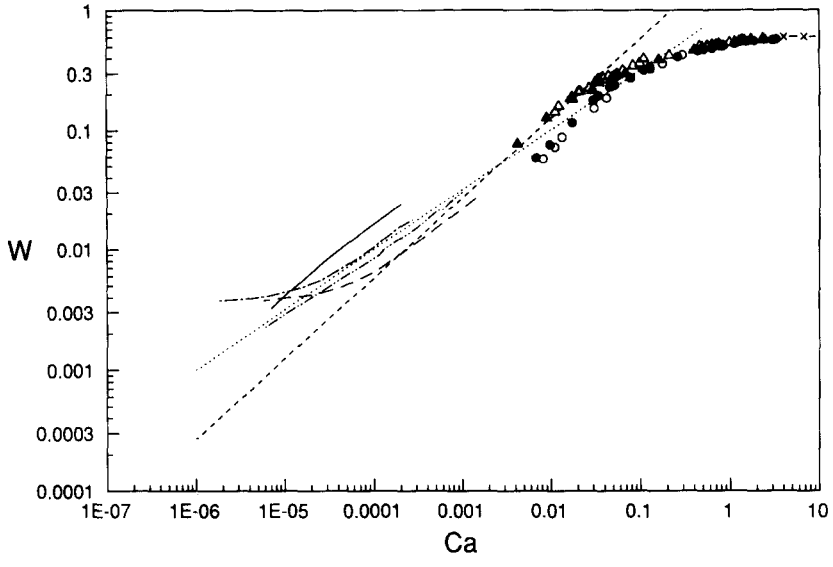

Fig. 7. Relative bubble velocity, W as a function of Capillary number for circular capillaries: (●) 1000 and 50 centistokes silicone oil, horizontal flow; (▲) 1000 and 50 centistokes silicone oil, upward flow; (○) 1000 and 50 centistokes silicone oil, downward flow. (△) 1000 and 50 centistokes silicone oil, bubble-train flow; (———) Marchessault and Mason's experimental results, (. . .) Fairbrother and Stubbs (1935) correlation; (– –) Brethertons (1961) correlation; (— –) Chen's (1986) experimental results for air bubble; (— —) Chen's (1986) experimental results for oil bubble; (— – –) Schwartz *et al.* (1986) experimental results; (— ×) Cox's (1961) asymptotic limit for W.

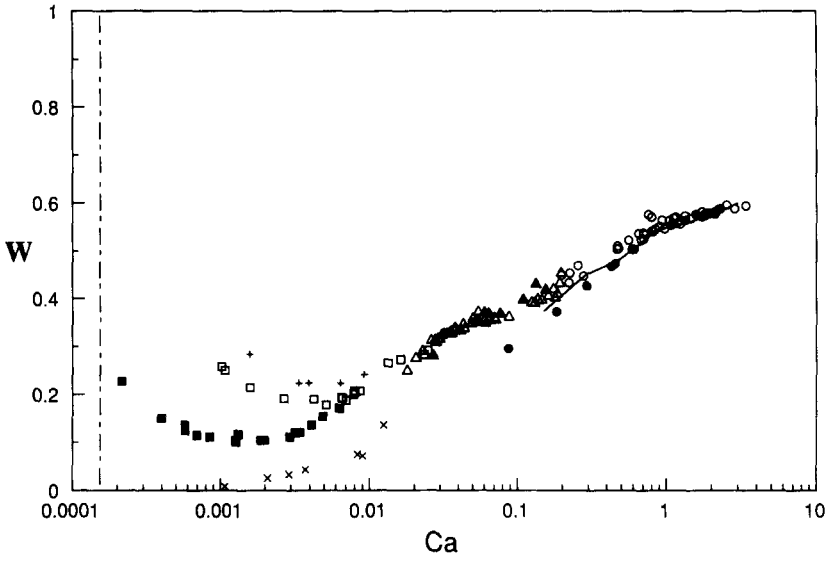

Fig. 8. Relative bubble velocity, W as a function of Capillary number for square capillaries: (●) 1000 centistokes silicone oil, downward flow; (○) 1000 centistokes silicone oil, bubble-train flow; (▲) 50 centistokes silicone oil, upward flow; (△) 50 centistokes silicone oil, bubble-train flow; (+) 5 centistokes silicone oil, upward flow; (×) 5 centistokes silicone oil, downward flow; (□) 5 centistokes silicone oil, bubble-train flow; (■) water, bubble-train flow. The solid line represents Kolb and Cerro (1991) experimental results for downward flow. The broken line represents the limiting Ca of 1.5×10^{-4} of a bubble inside a stagnant fluid in the square capillary.

found when the diameter of the bubble levels off and reaches a constant value (see Fig. 6). By further decreasing the liquid flow rate, the total flow rate decreases but the velocity of the bubble can never be smaller than the velocity of a bubble inside a stagnant fluid, as in the case when the capillary is sealed at one end. For this limiting case of a 50 centistoke silicone oil, the value of $W = 1.0$ and the capillary number $Ca = 1.5 \times 10^{-4}$. The Bond number for this case, $Bo = 0.43$, is lower than what is considered to be

a minimum ($Bo = 0.842$) for a bubble to be able to rise in a circular capillary. The flow at the corners of the square capillary provide an outlet for the liquid to move down and for the bubble to rise, even in small size capillaries. Though the diameters of air bubbles in water and 5 centistoke silicone oil are very close, the values of W are very different for low Ca. Again, the only explanation to these discrepancies can be found in the different flow rates at the corners.

Computation of flow parameters from gas and liquid superficial velocities

Flow parameters, such as the velocity of the bubbles and liquid slugs, the thickness of the liquid film surrounding the bubbles and the gas volume fraction inside the capillary cells, cannot be measured during the operation of the monolith reactor. Hence it is important to be able to compute these values using the gas and liquid flow rates or their corresponding superficial velocities. The functional dependence of bubble diameter and bubble cross-sectional area on Capillary number for circular and square capillaries has been analyzed experimentally. This functional dependence can now be used to solve the hydrodynamic model for bubble-train flow developed in Section 3.

The experimental data on the cross-sectional area of the bubble inside circular or square capillaries can be represented by third-order polynomials in $\ln(Ca)$. The film flow rate, q_{lf} can be calculated using eq. (17) or eq. (18). Next, eq. (15) and the third-order polynomials in $\ln(Ca)$ can be solved using a Newton–Raphson method with Ca as the iteration variable. An initial guess of Ca is used to start the computations and convergence was achieved in few iterations. The convergence criteria was set at 0.1% for all Ca. The total superficial velocity, J is the only input parameter needed for this solution.

Dimensionless bubble velocities, defined as U_b/J and computed using the procedure described here, are compared to experimental values for circular capillaries in Fig. 9. The agreement between experimental and computed values is within the range of experimental uncertainty in the measurement of gas and liquid flow rates. Although the results shown here are for bubble-train flow, they are also applicable to very long bubbles, that is bubbles with open back end. For low Ca dimensionless bubble velocities approach $U_b/J = 1$. In the upward flow regime the transition to complete bypass, that is when the velocity of the bubble is equal to the maximum velocity of the liquid slug, $U_b/J = 2$, is predicted for $Ca = 0.5$. For horizontal flow, bypass occurs at $Ca = 0.7$. This result agrees with the experimental result of $Ca = 0.7$ reported by Taylor (1961). For downward flow, transition occurs at $Ca = 0.6$. For large Ca the computational results level off to a limiting value of $U_b/J = 2.4$. It is interesting to compare this value with the limiting value predicted by eq. (6) for laminar flow of bubbles in large tubes: $U_b/J = 2.27$. Notice that for pipe flow the Capillary number dependence is meaningless and the comparison is simple between the bubble velocity and the overall superficial velocity.

Values of U_b/J for the square capillary are shown in Fig. 10. The agreement between the experiments and the model, eq. (15), is very good. The overall dependence of U_b/J with the Ca is very similar to the one found for circular capillaries, except at low Ca. The relative velocity between the bubble and the liquid slug increases with Ca and reach the maximum at about $Ca = 2.0$. For upward flow the transition to complete bypass, is predicted at $Ca = 0.50$. For downward flow the transition is predicted at $Ca = 0.57$. This is very close to the experimental value, $Ca = 0.60$, reported by Kolb and Cerro (1991). At low

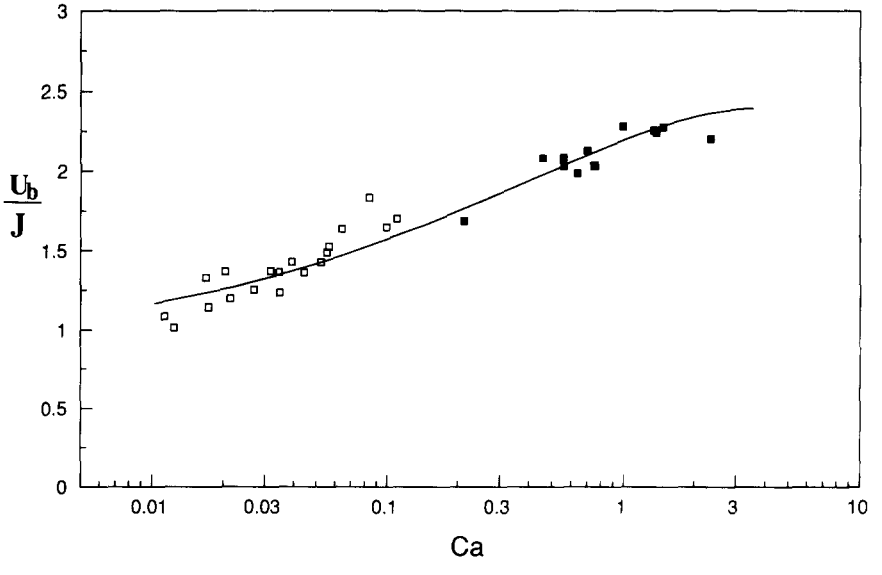

Fig. 9. Dimensionless bubble velocity defined as the ratio of bubble velocity to total superficial velocity for circular capillaries: (■) 1000 centistokes silicone oil, bubble-train flow; (□) 50 centistokes silicone oil, bubble-train flow. The solid line represents solution obtained from eq. (15).

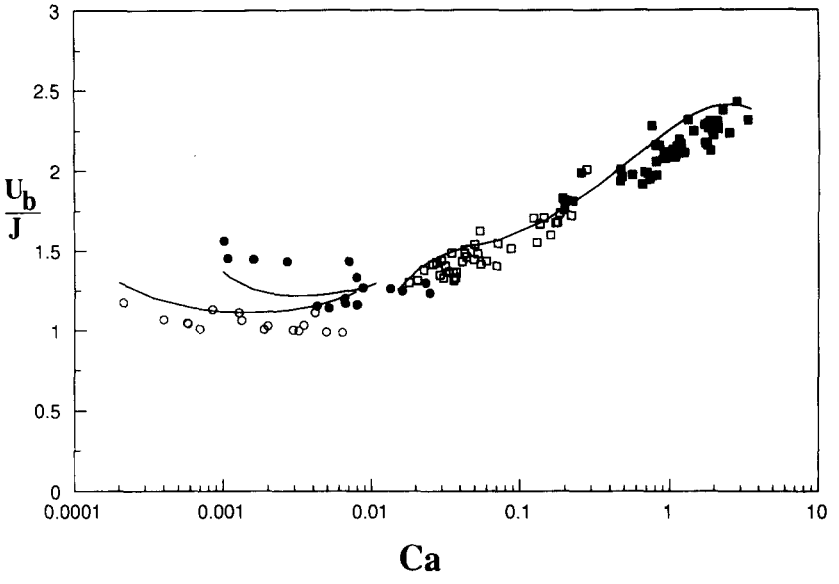

Fig. 10. Dimensionless bubble velocity defined as the ratio of bubble velocity to total superficial velocity for square capillaries: (■) 1000 centistokes silicone oil, bubble-train flow; (□) 50 centistokes silicone oil, bubble-train flow; (●) 5 centistokes silicone oil, bubble-train flow; (○) water, bubble-train flow. The solid line represents solution obtained from eq. (15).

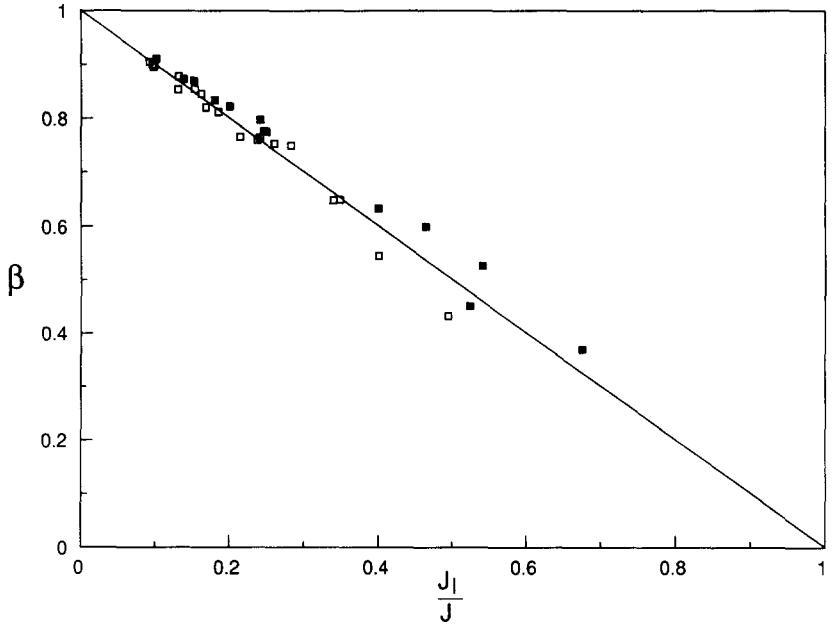

Fig. 11. Ratio of bubble length to unit cell length as a function of ratio of liquid flow rate to total flow rate for circular capillaries: (■) 1000 centistokes silicone oil, bubble-train flow; (□) 50 centistokes silicone oil, bubble-train flow. The solid line represents $(1 - J_l/J)$.

Ca, for both water and 5 centistoke silicone oil, the computed dimensionless bubble velocities reach a minimum compatible with the minimum experimental value of *W*.

The ratio of the length of the bubble to that of one unit cell, $\beta = (l_b + d_b)/l_T$ is an indication of the relative length of bubbles and liquid slugs, and is needed in order to compute mass transfer rates and pressure drop inside the capillary cells of the monolith. Pressure drop due to the movement of a unit cell can be computed assuming no pressure drop along the bubble body and viscous pressure drop in the liquid slug assuming a Poiseuille-like flow. Figure 11 shows experimental values of β for the circular capillary, compared with theoretical values computed using an approximation of eq. (20) where the term $d_b/3l_T$ has

been neglected. Under this approximation, theoretical values of β fall in a straight line defined by $\beta \approx 1 - J_l/J$. This approximation is valid if the gravity film flow, $q_{lf} \ll AJ$. In most cases this is a fair approximation. Theoretical values of β can be computed for every case using the complete form of eq. (20). The correction term, $(d_b/3l_T)$ varied in the range 0.088–0.016 for all the range of experimental data. Experimental values of β for the square capillary are shown in Fig. 12. In this case also, theoretical values are shown as a straight line given by the approximation $\beta \approx 1 - J_l/J$. Values of the correction term $d_b/3l_T$ varied between 0.09 and 0.012 for all cases. In order to demonstrate the effect of the correction term, for one of the experimental points the actual theoretical value (point 2) given by the complete form of eq. (20) is compared with the corresponding experimental data (point 1). The difference between the experimental value, $\beta_{exp} = 0.63$ and the theoretical value, $\beta_{th} = 0.54$, is within experimental error.

One of the most important parameters is the volume fraction of liquid inside the capillary cells, $1 - \alpha$. This parameter is needed in order to compute the residence time of liquid inside the monolith reactor (Patrick *et al.* 1994). Experimental values of $1 - \alpha$ for the circular capillary are shown in Fig. 13. Theoretical values of $1 - \alpha$ are shown as straight lines of constant Ca. Given the total superficial velocity, J, the velocity of the bubble, U_b, and in turn the Ca for a given gas–liquid system, are defined. The lines of constant Ca are also lines of constant J. The liquid volume fraction, approaches the upper limit $1 - \alpha = 1.0$ when the gas flow rate is zero. On the other hand, from eqs (14) and (15) it is possible to show that the lower limit for the liquid fraction, that is when $J_l = 0$ and $J = J_g$, is given by $1 - \alpha = (1 - A_b/A + q_{lf}/AU_b)$. As a consequence, the lower limit of $1 - \alpha$ depends on the value of Ca. The largest value of this lower limit is approached as $Ca \to \infty$ and is given by Cox's limit of $W = 0.6$. Indicated in Fig. 13 are the experimental Ca of two data points. It is possible to see that experimental data follows very closely the theoretical lines. Experimental values of $1 - \alpha$ as a function of J_l/J for the square capillary are shown in Fig. 14. For square capillaries lines of constant Ca are also lines of constant J. Shown in Fig. 14 are the lines for $Ca = 1.0, 0.1, 0.01$, and 0.001. In this case also, the largest possible value of the lower limit is given by Kolb and Cerro (1991) value of $W = 0.6$. Indicated in Fig. 14 are experimental values of Ca for two data points to demonstrate the dependence of the liquid volume fraction with Ca.

Missing in these computations are values of the film thickness surrounding the bubbles, measured in the direction normal to the wall, inside capillaries with square cross section. Data shown in Fig. 6 indicate that these films are very thin and their thickness decreases asymptotically as $Ca \to 0$. Because of their very small thickness, it is not feasible to measure directly the thickness of these films using a video-imaging system.

6. CONCLUDING REMARKS

The monolith reactor is an attractive, viable alternative for carrying out mass transfer limited reactions due to the large interfacial area caused by the gas–liquid flow patterns inside the reactor. The large interfacial area is due to the large number of bubbles separated by small liquid slugs. The very thin liquid

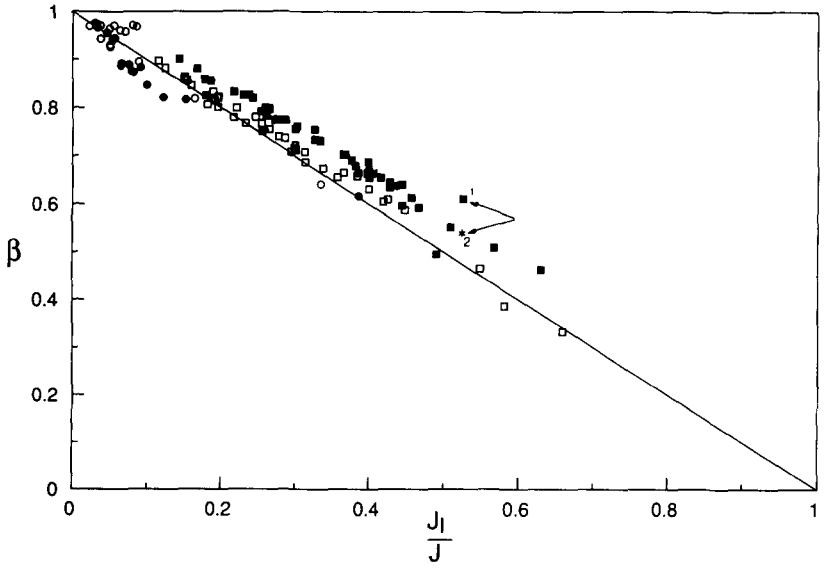

Fig. 12. Ratio of bubble length to unit cell length as a function of ratio of liquid flow rate to total flow rate for square capillaries: (■) 1000 centistokes silicone oil, bubble-train flow; (□) 50 centistokes silicone oil, bubble-train flow; (●) 5 centistokes silicone oil, bubble-train flow; (○) water, bubble-train flow. The solid line represents $(1 - J_l/J)$. Point 1 is the experimental point. Point 2 is calculated using eq. (20).

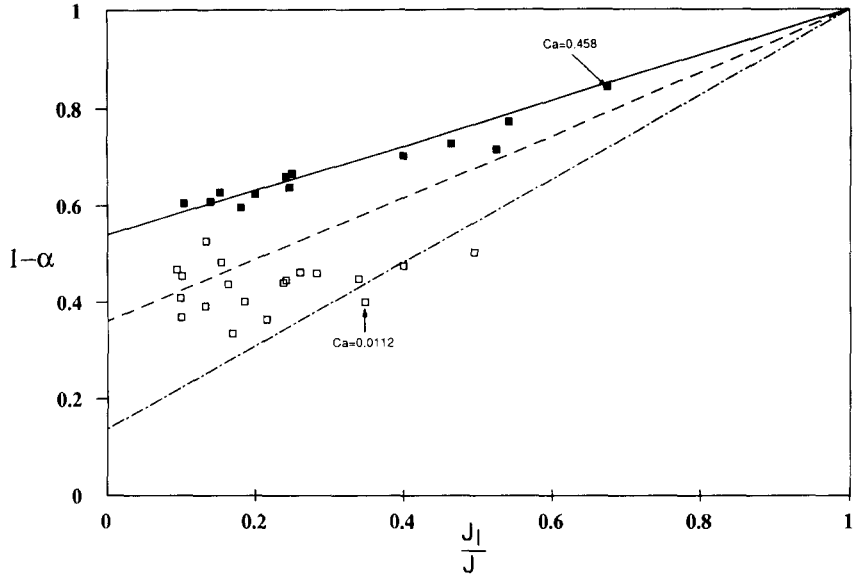

Fig. 13. Volume fraction of liquid as a function of ratio of liquid flow rate to total flow rate for circular capillaries: (■) 1000 centistokes silicone oil, bubble-train flow; (□) 50 centistokes silicone oil, bubble-train flow. The lines are drawn at constant *Ca*; (———) $Ca = 1.0$; (— —) $Ca = 0.10$; (— –) $Ca = 0.01$.

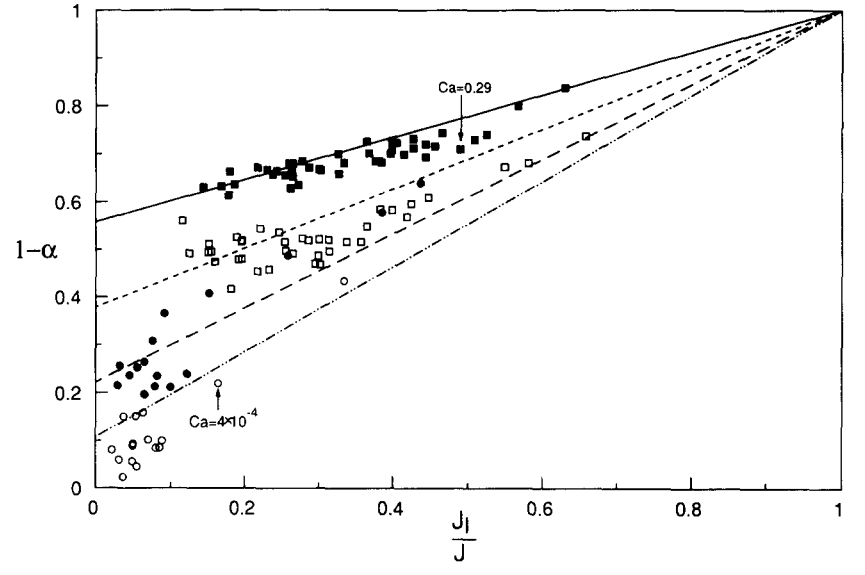

Fig. 14. Volume fraction of liquid as a function of ratio of liquid flow rate to total flow rate for square capillaries: (■) 1000 centistokes silicone oil, bubble-train flow, (□) 50 centistokes silicone oil, bubble-train flow; (●) 5 centistokes silicone oil, bubble-train flow. (○) water, bubble-train flow. The lines are drawn at constant *Ca*: (———) $Ca = 1.0$; (– –) $Ca = 0.10$; (— —) $Ca = 0.01$; (— – –) $Ca = 0.001$.

film surrounding the bubble offers minimum resistance to mass transfer from the gas to the liquid and to the solid monolith wall. The liquid film is continuously regenerated and remains stable despite its very small thickness. The convective patterns within the liquid slug, generated by the relative movement of the bubbles with respect to the liquid slugs, enhances mixing inside the liquid phase. These unique features makes the monolith reactor ideal for mass transfer limited reactions.

To provide a basis for these claims some typical mass transfer parameters have been computed from experimental observations and are shown in Table 1. The gas–liquid interfacial area as well as the liquid film thickness were estimated from experimental data for circular and square capillaries for several relevant

Table 1. Interfacial gas–liquid mass transfer area and liquid film thickness for capillaries of circular and square cross section

Fluid	Superficial liquid velocity (m/s) × 10^2	Superficial gas velocity (m/s) × 10^2	Ca	Re	β	Interfacial area per unit volume (m^2/m^3)	Film thickness × 10^6 m
Circular capillary (2 mm *ID*)							
1000 oil	0.34	1.02	1.34	0.0612	0.77	1036	332
"	0.15	0.46	0.56	0.0256	0.77	1106	286
"	0.34	0.29	0.557	0.0254	0.526	743	294
50 oil	0.28	0.79	0.032	0.59	0.75	1316	126
"	0.17	0.42	0.017	0.313	0.75	1362	91
"	0.28	0.42	0.0172	0.317	0.545	988	94
Square capillary (2 mm *size*)							
1000 oil	0.47	1.17	1.11	0.0507	0.664	780	253
"	0.21	0.34	0.47	0.021	0.66	840	196
"	0.36	0.83	1.10	0.0502	0.756	900	242
50 oil	0.73	1.91	0.087	1.603	0.74	1066	81
"	0.37	0.94	0.043	0.792	0.74	1089	59
"	0.41	0.91	0.041	0.755	0.708	1056	51
"	0.41	0.34	0.022	0.405	0.46	709	47
5 oil	0.29	8.4	0.023	44.0	0.967	1482	—
"	0.29	5.97	0.016	30.6	0.96	1479	—
Water	1.70	44.2	0.006	862.3	0.97	1589	—
"	0.20	8.76	0 0013	186.8	0.97	1665	—
"	0.44	7.78	0.0012	172.4	0.94	1622	—

flow rates. The film thickness of the bubble in the axial plane, for 5 centistoke silicone oil and for water, were neglected in these calculations. The gas–liquid interfacial area varied from 700 to 1500 m^2/m^3 based on the volume of the monolith channels. To translate this ratio to the total reactor volume one needs to multiply the specific area by the open flow area (OFA) of the monoliths. For a 200/12 monoliths the OFA = 69%. The specific area, for a constant ratio of gas to liquid flow rate, increases with decreasing Ca. The thickness of the film surrounding the bubble, for constant gas to liquid flow rate, decreases with decreasing Ca. For the typical operating range of flow rates encountered in the experimental monolith foam reactor, the gas–liquid interfacial area is in the order of 1500 m^2/m^3.

The computational method and the experimental results presented here can be used to determine the mass transfer parameters necessary to estimate the performance of one capillary cell. During the actual operation of the monolith foam reactor, these flow rates and mass transfer performance may vary from cell to cell and average values of the mass transfer parameters must be used.

Acknowledgements—The support of the National Science Foundation through grant CTS-9022241 and amendment CTS-9247166, is gratefully acknowledged. The authors are also grateful for the support of the Office of Research of The University Tulsa and the Associate Dean for Research of the College of Engineering and Applied Sciences.

NOTATION

a	half-width of square capillary, m
A	area, m^2
A_b	bubble cross-sectional area, m^2
Bo	Bond number ($= \varrho g R^2/\sigma$)
Ca	Capillary number ($= \mu U_b/\sigma$)
C, C_1, C_2	constants
d_b	diameter of the hemispherical cap of the bubble, m
D	diameter of tube or capillary, m
D_b	dimensionless bubble diameter
g	acceleration due to gravity, m/s^2
J	total flow rate across the capillary cross section, m/s
J_g	gas flow rate across the capillary cross section, m/s
J_l	liquid flow rate across the capillary cross section, m/s
l_b	length of uniform film region of the bubble, m
l_s	length of liquid slug, m
l_T	length of unit cell made of a bubble and liquid slug, m
n_D	refractive index
q_{lf}	flow rate of liquid in the film, m^3/s
r	radial coordinate, m
R	radius of the circular capillary, m
Re	Reynolds number ($= \varrho v D/\mu$)
R_b	radius of the bubble, m
R_s	dimensionless bubble radius
$R_{S(A-A)}$	bubble radius in side plane, m
$R_{S(B-B)}$	bubble radius in diagonal plane, m
t_b, t_T	time elapsed defined by eq. (9), s
U_b	bubble velocity, m/s
V_g	volume of bubble, m^3
V_l	volume of liquid, m^3
v_{ls}	mean velocity in the liquid slug, m/s
v_z	velocity of liquid in the film, m/s

W velocity ratio for fraction of liquid deposited on walls

Greek letters

α volume fraction of liquid inside the capillary

β ratio of bubble length to length of one unit cell

μ_l viscosity of liquid phase, Pa s

ϱ_l density of liquid phase, kg/m^3

σ interfacial tension, mN/m

REFERENCES

Ariga, O., Kimura, M., Taya, M. and Kobayashi, T., 1986, Kinetic evaluation and characterization of ceramic honeycomb-monolith bioreactor. *J. Ferment. Technol.* **64**, 327–334.

Bendiksen, K. H., 1985, On the motion of long bubbles in vertical tubes. *Int. J. Multiphase flow* **11**, 797–812.

Benoit, M. R. and Kohler, J. T., 1975, An evaluation of a ceramic monolith as an enzyme support material. *Biotech. Bioeng.* **XVII**, 1617–1626.

Bretherton, F. P., 1961, The motion of long bubbles in tubes. *J. Fluid Mech.* **10**, 166–188.

Chen, J. D., 1986, Measuring the film thickness surrounding a bubble inside a capillary. *J. Colloid Interface Sci.* **109**, 341–349.

Collins, R., Morases, F. F. D., Davidson, J. F. and Harrison, D., 1978, The motion of a large gas bubble rising through liquid flowing in a tube. *J. Fluid Mech.* **89**, 497–514.

Cox, B. G., 1962, On driving a viscous fluid out of a tube. *J. Fluid Mech.* **14**, 81–96

Cox, B. G., 1964, An experimental investigation of the streamlines in viscous fluid expelled from a tube. *J. Fluid. Mech.* **20**, 193–200.

Crynes, L. L., Cerro, R. L. and Abraham, M., 1994, The monolith froth reactor: development of a novel three-phase catalytic system. *A.I.Ch.E. J.* (accepted).

Davies, R. M. and Taylor, G. I., 1950, The mechanics of large bubbles rising through extended liquids and through liquids in tubes. *Proc. Roy. Soc.* **A200**, 375–390.

Fairbrother, F. and Stubbs, A. E., 1935, Studies in electro-endosmosis—VI. The "bubble tube" method of measurement. *J. chem. Soc.* **1**, 527–529.

Goldsmith, H. L. and Mason, S. G., 1963, The flow of suspensions through tubes—II. Single large bubbles. *J. Colloid Interface Sci.* **18**, 237–261.

Herbolzheimer, E., 1987, The effect of surfactants on the motion of a bubble in a capillary. *A.I.Ch.E Annual Meeting*, November 15–20, New York, paper 68j.

Irandoust, S. and Gahne, O., 1990, Competitive hydrodesulfurization and hydrogenation in a monolith reactor. *A.I.Ch.E. J.* **36**, 746–752.

Kawakami, K., Kawasaki, K., Shiraishi, F. and Kusunoki, K., 1989, Performance of a honey-comb monolith bioreactor in a gas–liquid–solid three phase system. *Ind. Engng Chem. Res.* **28**, 394–400.

Kolb, W. B. and Cerro, R. L., 1991, Coating the inside of a capillary of square cross section. *Chem. Engng Sci.* **46**, 2181–2195.

Kolb, W. B. and Cerro, R. L., 1993a, The motion of long bubbles in tubes of square cross section. *Phys. Fluids* **A 5**, 1549–1557.

Kolb, W. B. and Cerro, R. L., 1993b, Film flow in the space between a circular bubble and a square tube. *J. Colloid Interface Sci.* **159**, 302–311.

Marchessault, R. N. and Mason, S. G., 1960, Flow of entrapped bubbles through a capillary. *Ind. Eng. Chem.* **52**, 79–84.

Martinez, M. J. and Udell, K. S., 1989, Boundary integral analysis of the creeping flow of long bubbles in capillaries, *J. appl. Mech.* **56**, 211–217.

Patrick, R., Klindera, T., Crynes, L. L., Cerro, R. L. and Abraham, M. A., 1994, Residence time distribution inside a monolith froth reactor. *A.I.Ch.E. J.* (accepted).

Pozrikidis, C., 1992, The buoyancy driven motion of a train of viscous drops within a cylindrical tube. *J. Fluid Mech.* **237**, 627–648.

Ramos, A. Lopez de, R. A. Redner and R. L. Cerro, 1994, Surface tension from pendant drop curvature. *Langmuir* (accepted).

Ratulowski, J. and Chang, H. C., 1989, Transport of gas bubbles in capillaries. *Phys. Fluids* **A 1**, 1642–1655.

Ratulowski, J. and Chang, H. C., 1990, Marangoni effects of trace impurities on the motion of long gas bubbles in capillaries. *J. Fluid Mech.* **210**, 303–328.

Reinelt, D. A., 1987, The rate at which a long bubble rises in a vertical tube. *J. Fluid Mech.* **175**, 557–565.

Reinelt, D. A. and Saffman, P. G., 1985, The penetration of a finger into a viscous fluid in a channel and tube. *J. Sci. Statist. Comput.* **6**, 542–561.

Satterfield, C. N. and Ozel, F., 1977, Some characteristics of two-phase flow in monolithic catalyst structures. *Ind. Eng. Chem. Fundam* **16**, 61–67.

Schwartz, L. W., Princen, H. M. and Kiss, A. D., 1986, On the motion of bubbles in capillary tubes. *J. Fluid Mech.* **172**, 259–275.

Shah, Y. T., Abraham, M. A. and Cerro, R. L., 1993, Oxidation of phenol in a three-phase monolithic froth reactor, in *Three-Phase Sparged Reactors* (Edited by K. D. P. Nigam and A. Schumpe) Gordon and Breach, New York.

Shen, E. I. and Udell, K. S., 1985, A finite element study of low Reynolds number two-phase flow in cylindrical tubes. *J. appl. Mech.* **52**, 253–256.

Taylor, G. I., 1961, Deposition of a viscous fluid on the wall of a tube. *J. Fluid Mech.* **10**, 161–165.

Teletzke, G. F., 1983, Thin liquid films: molecular theory and hydrodynamic implications. Ph.D. thesis. Department of Chemical Engineering, University of Minnesota.

Wallis, G. B., 1969, *One-Dimensional Two-Phase Flow.* McGraw-Hill, New York.